

In-beam γ -ray spectroscopy above ^{100}Sn using the new technique of recoil decay tagging

E. S. Paul,² P. J. Woods,¹ T. Davinson,¹ R. D. Page,¹ P. J. Sellin,¹ C. W. Beausang,² R. M. Clark,³ R. A. Cunningham,⁴ S. A. Forbes,² D. B. Fossan,⁵ A. Gizon,⁶ J. Gizon,⁶ K. Hauschild,³ I. M. Hibbert,³ A. N. James,² D. R. LaFosse,⁵ I. Lazarus,⁴ H. Schnare,⁵ J. Simpson,⁴ R. Wadsworth,³ and M. P. Waring⁵

¹Department of Physics, University of Edinburgh, Edinburgh EH9 3JZ, United Kingdom

²Oliver Lodge Laboratory, University of Liverpool, PO Box 147, Liverpool L69 3BX, United Kingdom

³Department of Physics, University of York, Heslington, York YO1 5DD, United Kingdom

⁴SERC Daresbury Laboratory, Daresbury, Warrington WA4 4AD, United Kingdom

⁵Department of Physics, State University of New York at Stony Brook, New York 11794

⁶Institut des Sciences Nucléaires, IN2P3-CNRS/Université Joseph Fourier, Grenoble, France

(Received 26 August 1994)

A novel method of selecting γ -ray transitions in heavy nuclei ($A > 100$) at the proton drip-line has been attempted. The characteristic charged-particle radioactivity of these nuclei (alpha decay, ground-state proton decay, and β -delayed proton emission) has been used to tag γ -ray transitions recorded by the highly efficient Eurogam spectrometer. The $^{58}\text{Ni} + ^{54}\text{Fe}$ and $^{58}\text{Ni} + ^{58}\text{Ni}$ fusion-evaporation reactions, at a beam energy of 240 MeV, have been used to populate specific states of these neutron-deficient nuclei and results are presented for $^{108,109}\text{Te}$, ^{109}I , and ^{113}Xe , where γ -ray transitions have been identified. In the case of ^{109}I , this represents the first observation of γ -rays from a ground-state proton emitter.

PACS number(s): 21.10.Re, 27.60.+j, 23.20.Lv

I. INTRODUCTION

In the past decade much progress has been made in extending the systematics of nuclei near $N = Z$ (e.g., Ref. [1]). A typical approach is to use a high-efficiency γ -ray detector array in conjunction with a recoil mass separator [1]. The mass A of a fusion-evaporation residue is identified by its position at the focal plane and its charge Z from energy-loss characteristics in an ionization chamber. For high Z (≥ 50), the identification becomes increasingly difficult for slow-moving evaporation residues and isobaric contamination becomes a serious problem. One alternative approach to this problem, reported by the Nordball collaboration [2,3], is to surround the target with a multidetector array of silicon detectors and liquid scintillators in order to identify evaporation protons, alpha particles, and neutrons. In the present paper, we report on the novel method of recoil decay tagging (RDT) and have used the technique to identify γ rays from extremely neutron-deficient isotopes in the region above ^{100}Sn .

II. METHOD OF RECOIL DECAY TAGGING

Many of the nuclei in the region above ^{100}Sn decay by emitting characteristic alphas, β -delayed protons, and direct protons from their ground states (e.g., Ref. [4]). These charged-particle decay modes offer a unique signature that a given state of a particular isotope has been produced and can be efficiently detected by implanting evaporation residue ions inside a silicon detector. A

schematic diagram of the apparatus used in recoil decay tagging (RDT) is shown in Fig. 1. A highly sensitive technique has been developed by the Edinburgh group to identify weakly produced proton-radioactive nuclei using a double-sided silicon strip detector (DSSD)

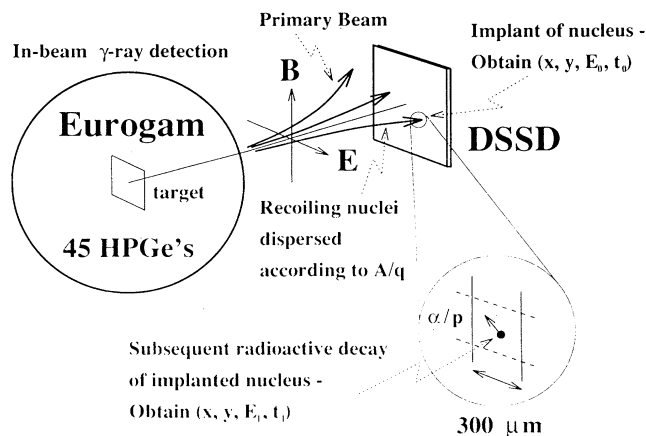


FIG. 1. Schematic diagram showing the principle of recoil decay tagging. Prompt γ rays are recorded by Eurogam. Recoiling evaporation residues pass through a velocity filter with crossed electric (E) and magnetic (B) fields (Daresbury Recoil Separator) and are dispersed according to their mass-to-charge ratio (A/q) before being implanted into the double-sided silicon strip detector (DSSD) at position (x, y) at time t_0 with energy E_0 . Within the same pixel (x, y) , subsequent charged-particle radioactivity (decay at time t_1 with energy E_1) can be correlated with the initial implantation.

[5]. In these experiments, ions that have been velocity and mass analyzed by the Daresbury Recoil Separator [6] were implanted into the DSSD and the position, time, and energy of the ions (x_0, y_0, t_0, E_0) and subsequent decays (x_1, y_1, t_1, E_1) were recorded. The high degree of DSSD segmentation (48×48 strips) ensured an efficient correlation between implantations and decays occurring in the same pixel ($x_1 = x_0, y_1 = y_0$). These implanted ions also pass through a carbon-foil channel plate detector before entering the DSSD. Signals from the channel plate detector can be used to provide position-mass information on the ions and to provide a fast delayed coincidence between the recoil separator focal plane and γ rays detected around the target [1,6]. One can therefore in principle establish a link between delayed radioactive decays occurring in the DSSD at the focal plane with in-beam γ rays emitted at the target position. In the next section, the first experiments using the RDT method are reported.

III. EXPERIMENTAL DETAILS AND RESULTS

In the penultimate month of running experiments at the Nuclear Structure Facility, Daresbury, the opportunity became available to parasite on an experiment using the Eurogam γ -ray detector array, consisting of 45 large-volume escape-suppressed HPGe detectors with a total photopeak efficiency of 4.5% ($E_\gamma = 1.33$ MeV) [7,8]. The Eurogam array was situated on the recoil separator beam line offering the unique opportunity of coupling together Eurogam, the Daresbury recoil separator, and the Edinburgh DSSD. In the experiment, data were recorded by two parallel data-acquisition systems to avoid compromising the main experiment. All decay and implantation events were written to tape by one system including the time at which each event occurred (generated by a 32-bit pattern register and scalar driven at a clock frequency of 100 kHz [5]). The second acquisition system wrote events to tape containing recoil- γ^n events ($n \geq 1$) in which all suppressed HPGe detectors present in prompt coincidence (50 ns) were recorded together with signals taken from the channel-plate detector. In addition, a time word was also written to those events that corresponded to transient evaporation residues implanting into the DSSD with at least one γ ray detected. This time word was common to both data sets and could be used to link a single evaporation residue event recorded in each data set. During off-line analysis, radioactive decays from the first data set could be correlated with evaporation residues, and from the common time information these events could in turn be identified with γ rays recorded in the second data set in fast coincidence with evaporation residues. An additional tape was written containing only pure γ -ray data in which Compton-suppressed events were recorded with a trigger requirement of at least six unsuppressed HPGe detectors firing in prompt coincidence.

A. $^{58}\text{Ni} + ^{54}\text{Fe}$ reaction

The Daresbury tandem Van de Graaff accelerator provided a 240-MeV ^{58}Ni heavy-ion beam to bombard a thin ($500 \mu\text{g}/\text{cm}^2$) self-supporting ^{54}Fe target in order to produce the compound nucleus $^{112}\text{Xe}^*$ with an excitation energy ~ 57 MeV. The beam current of 3–4 particle nA led to an individual HPGe detector rate of 6–7 kHz while the DSSD event rate was ~ 1 kHz. The dominant nuclei produced were ^{109}Sb (via the $3p$ exit channel [9]), ^{108}Sb ($3pn$ [3]), ^{108}Sn ($4p$ [10]), and ^{106}Sn ($\alpha 2p$ [11]). This reaction would also be expected to produce the α -decaying nuclei ^{108}Te ($E_\alpha = 3.32$ MeV, $t_{1/2} = 2.1$ s, $b_\alpha = 0.49$ [12,13,4]) via the $2p2n$ exit channel and ^{109}Te ($E_\alpha = 3.11$ MeV, $t_{1/2} = 4.1$ s, $b_\alpha = 0.039$ [12–14]) via the $2pn$ channel. In the case of ^{109}Te , a β -delayed proton branch also occurs ($E_p \sim 2$ –5 MeV, $b_{\beta p} = 0.094$ [15,16]). In addition, the proton-radioactive nucleus ^{109}I ($E_p = 0.81$ MeV, $t_{1/2} = 100 \mu\text{s}$, $b_p \sim 1.00$ [17,18]) should also be produced via the $p2n$ channel with a much smaller cross section. Figure 2 shows the $A = 108$ and 109 gated decay energy spectrum clearly revealing the presence of all these activities.

1. ^{108}Te

The nucleus ^{108}Te is a good test case to try the RDT method since it is an even-even nucleus and presumably all the cascade intensity should feed through the $2^+ \rightarrow 0^+$ transition. Figure 3(a) shows an $A = 108$ gated γ -ray spectrum and beneath it in Fig. 3(b) are those γ rays for which a ^{108}Te α decay occurred in the same DSSD pixel following implantation. It can be clearly seen that the structures of the two spectra are not the same, indicating that the correlation is selectively picking out transitions associated with ^{108}Te . However, the strong γ -ray lines from the $A = 108$ spectrum in Fig. 3(a) do contaminate the lower spectrum in Fig. 3(b). These events arise due

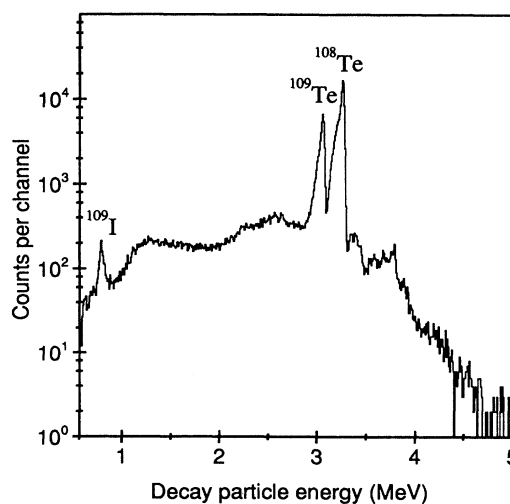


FIG. 2. Charged-particle decay energy spectrum obtained for the $^{58}\text{Ni} + ^{54}\text{Fe}$ reaction.

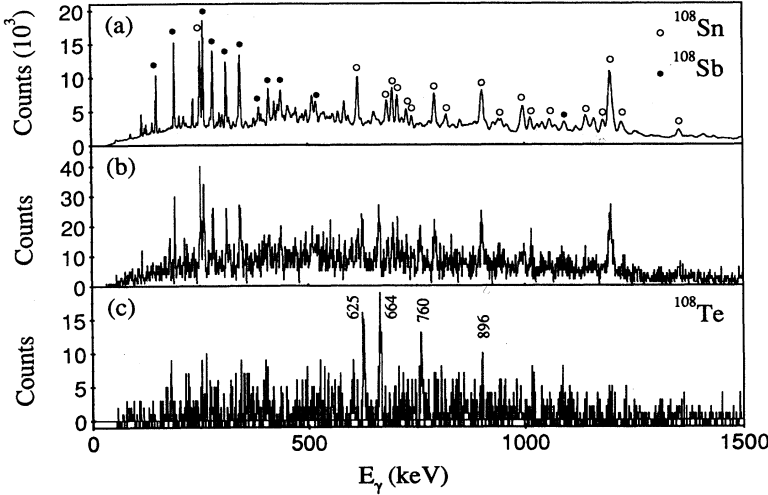


FIG. 3. (a) Mass-gated ($A = 108$) γ -ray spectrum with the strong transitions from ^{108}Sn and ^{108}Sb indicated. (b) Gamma rays correlated with the α decay of ^{108}Te . (c) Spectrum (b) minus a normalized fraction of spectrum (a) with the ^{108}Te transitions labeled by their energies in keV.

to false correlations between implanted ions and decays which occur due to the high implantation rate in the DSSD as a whole; the associated pixel rate of ~ 1 Hz is comparable to the decay rate of ^{108}Te ($t_{1/2} = 2.1$ s). In fact, only $\sim 25\%$ of the ^{108}Te α decays are correctly correlated with the parent implanted ion. The isobaric contaminant peaks can, however, be subtracted off to clearly reveal the ^{108}Te transitions shown in Fig. 3(c).

Four peaks of energies 625, 664, 760, and 896 keV are evident in Fig. 3(c). It has been possible to estab-

lish that these four transitions are in mutual coincidence by analysis of the recoil- γ - γ data; the ESCL8R graphical analysis code [19] has been used to analyze a mass-gated ($A = 108$) γ - γ matrix. Moreover, another γ ray of energy 998 keV appears to be in coincidence with the 625-664-760-896 keV sequence. We thus propose a decay scheme for ^{108}Te as shown in Fig. 4. An estimate of the relative population of this structure is approximately 0.25% of the intensity of the strongest reaction channel ($3p$ into ^{109}Sb). The weakness rules out any possible angular-correlation analysis and hence the spin-parity assignments in Fig. 4 are tentative. Table I lists the energies and relative intensities of the ^{108}Te transitions.

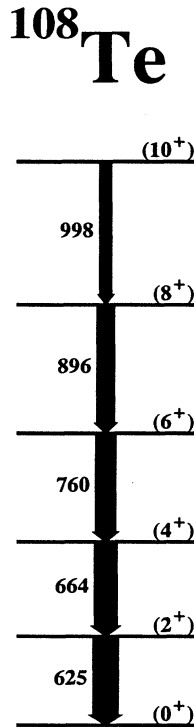


FIG. 4. Proposed decay scheme for ^{108}Te . Transition energies are given in keV and spin-parity assignments are tentative.

2. ^{108}Te

In the case of ^{109}Te , correlations can be performed with both alphas and β -delayed protons. Figures 5(a)–5(c) show, respectively, the $A = 109$ gated γ rays, the decay-tagged γ -ray spectrum, and the resulting subtracted spectrum showing γ rays from ^{109}Te . For ^{109}Te , only 0.133 of the decays are by either alpha or delayed proton emission and of these only $\sim 13\%$ will be correctly correlated to parent ^{109}Te implanted ions. Peaks are evident at 327, 495, 609, and 696 keV in Fig. 5(c) which we assign to ^{109}Te . One can hope to improve the statistics by gating on a clear line, such as the 327 keV transition,

TABLE I. Gamma-ray energies and intensities for transitions assigned to ^{108}Te .

E_γ (keV) ^a	I_γ (%) ^b
625.4	100
663.8	100
760.1	100
896.3	80
997.6	50

^aEnergies are accurate to ± 0.5 keV.

^bIntensities are accurate to $\pm 15\%$.

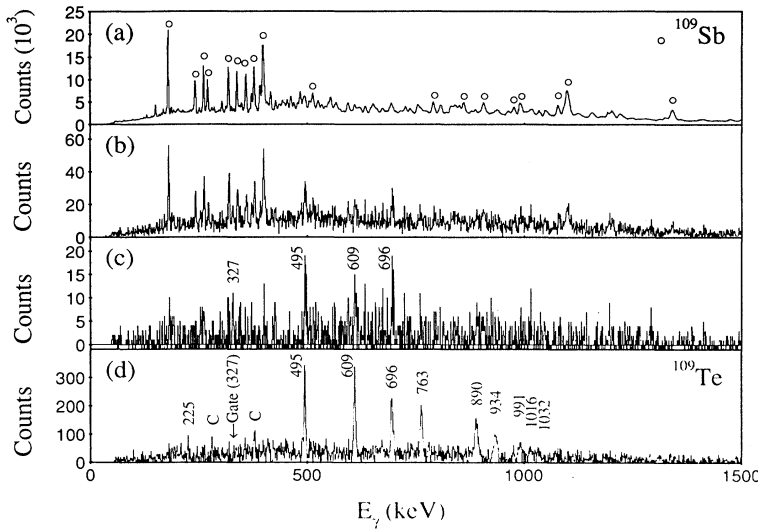


FIG. 5. (a) Mass-gated ($A = 109$) γ -ray spectrum with the strong transitions from ^{109}Sb indicated. (b) Gamma rays correlated with both the α decay and β -delayed proton decay of ^{109}Te . (c) Spectrum (b) minus a normalized fraction of spectrum (a) with the ^{109}Te transitions labeled by their energies in keV. (d) Gamma rays in coincidence with the 327 keV transition obtained from a mass-gated ($A = 109$) γ - γ matrix. The transitions assigned to ^{109}Te are labeled by their energies, while peaks labeled C are known contaminants.

in the recoil- γ - γ data. Figure 5(d) shows γ rays in coincidence with the 327 keV transition which clearly enhances the ^{109}Te peak structure compared to Fig. 5(c). Therefore, even with low decay branches one can recover high in-beam statistics provided at least one clear transition is identified.

Analysis of the recoil- γ - γ data ($A = 109$) resulted in the decay scheme shown in Fig. 6. Transition energies and intensities are listed in Table II. The ordering of the transitions is based on measured relative intensities of the γ rays; some transitions, however, have similar intensities. An estimate of the relative intensity of ^{109}Te is approximately 1% of that of the strongest reaction channel. From the pure γ -ray data set, it proved possible to extract angular correlation ratios $I_\gamma(134^\circ, 90^\circ)/I_\gamma(90^\circ, 134^\circ)$ for the majority of the new ^{109}Te transitions and thus to establish relative spin-parity values using the method of directional correlation from oriented states (DCO) [20]; the results are included in Table II. We have assigned absolute spin-parity values based on systematics; in particular a band based on an $11/2^-$ state is expected. We thus suggest $5/2^+$ for the ground state of ^{109}Te .

3. ^{109}I

For the case of the proton emitter ^{109}I , we expect low statistics and in fact 650 proton decays were identified in the DSSD at this nonoptimal beam current and energy over a period of 21 h (this corresponds to a cross section of $\sim 3 \mu\text{b}$ assuming a recoil separator efficiency $\sim 3\%$, which is to be compared with an optimal cross section of $50 \mu\text{b}$ measured at a lower beam energy of 229 MeV [21]). However, the half-life of $100 \mu\text{s}$ is extremely short and there should be essentially no isobaric contamination caused by false recoil-decay correlations. Figures 7(a) and 7(b) show the $A = 109$ γ -ray spectrum and those events correlated with ^{109}I protons, respectively. As expected, there is no evidence for the strongest isobaric transitions in Fig. 7(b), indicating that the spectrum is

effectively clear of contamination and no subtraction is therefore necessary. There is evidence for peak structure in Fig. 7(b) although the statistics are poor. By gating on these peaks in the recoil- γ - γ data ($A = 109$), the lines at 505, 514, 554, 596, 729, and 1074 keV do appear to be in coincidence with each other. The 505-596-729 keV transitions appear to form a band structure,

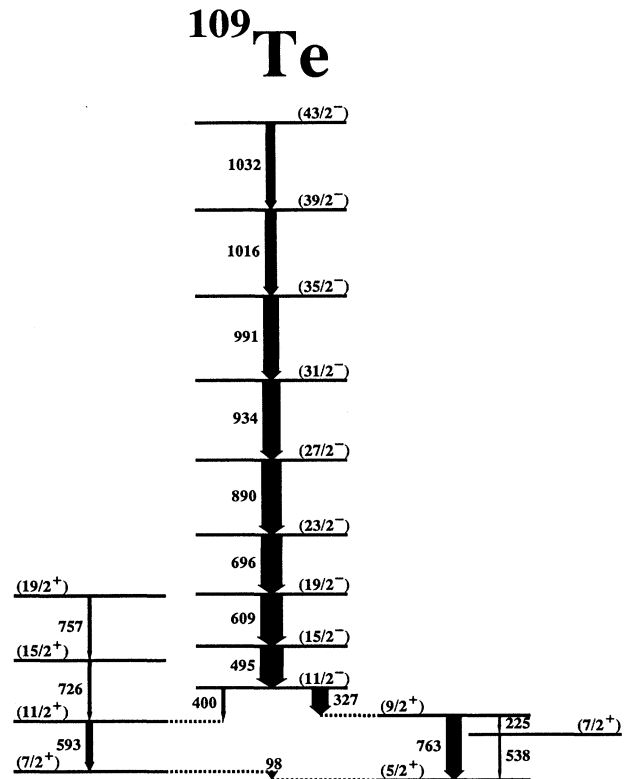


FIG. 6. Proposed decay scheme for ^{109}Te . Transition energies are given in keV and spin-parity assignments are tentative.

TABLE II. Gamma-ray energies, intensities, and angular correlation results for transitions assigned to ^{109}Te .

E_γ (keV) ^a	I_γ (%) ^b	$\frac{I_\gamma(134^\circ, \tilde{90}^\circ)^c}{I_\gamma(90^\circ, 134^\circ)}$	Multipolarity	Assignment
97.8	< 10	0.7(1)	$M1/E2$	$(7/2^+ \rightarrow 5/2^+)$
225.1	< 10	0.6(1)	$M1/E2$	$(9/2^+ \rightarrow 7/2^+)$
327.3	29	0.6(1)	$E1$	$(11/2^- \rightarrow 9/2^+)$
399.6	-d-		$(E1)$	$(11/2^- \rightarrow 11/2^+)$
494.6	$\equiv 100$	1.1(1)	$E2$	$(15/2^- \rightarrow 11/2^-)$
538.0	< 10	—	$(M1/E2)$	$(7/2^+ \rightarrow 5/2^+)$
593.0	14	1.0(1)	$E2$	$(11/2^+ \rightarrow 7/2^+)$
609.4	95	1.1(1)	$E2$	$(19/2^- \rightarrow 15/2^-)$
695.5	94	1.2(1)	$E2$	$(23/2^- \rightarrow 19/2^-)$
726.4	12	—	$(E2)$	$(15/2^+ \rightarrow 11/2^+)$
757.2	10	—	$(E2)$	$(19/2^+ \rightarrow 15/2^+)$
763.3	32	1.2(1)	$E2$	$(9/2^+ \rightarrow 5/2^+)$
889.9	90	1.0(1)	$E2$	$(27/2^- \rightarrow 23/2^-)$
933.9	90	1.1(1)	$E2$	$(31/2^- \rightarrow 27/2^-)$
990.9	84	1.0(1)	$E2$	$(35/2^- \rightarrow 31/2^-)$
1016.1	70	—	$(E2)$	$(39/2^- \rightarrow 35/2^-)$
1032.0	35	—	$(E2)$	$(43/2^- \rightarrow 39/2^-)$

^aEnergies are accurate to ± 0.5 keV.

^bIntensities are accurate to $\pm 10\%$.

^cEurogam contains ten detectors at $\theta=134^\circ$ and ten detectors at $\theta=\tilde{90}^\circ$ (five at 86° and five at 94°). Values ≥ 1.0 indicate stretched quadrupole transitions, while values ≈ 0.65 are expected for a pure stretched dipole.

^dDoublet with a strong transition in ^{109}Sb .

together with weaker 845 keV and 908 keV transitions, not visible in Fig. 7(b). Moreover, transitions of energies 373 keV, 514 keV, 554 keV, 868 keV, and 1074 keV are in coincidence with this sequence. Most of the latter transitions are not mutually coincident and thus probably depopulate the band structure via parallel pathways. The statistics are, however, too poor for any complete level scheme to be deduced with certainty. We may, however, conclude that the 505-596-729-845-908 keV band structure lies at least 1074 keV above the ground state of ^{109}I which, from systematics, suggests that this band is based on an $h_{11/2}$ proton orbital (see Fig. 14 later). It is noteworthy that the ^{109}I results represent the first γ -ray data from a ground-state proton emitter; indeed data have not yet even been published on the neighboring $^{110-112}\text{I}$ isotopes. The ^{109}I data provide the first direct informa-

tion on the feeding of a proton-unbound ground state and show that, as high as 4.6 MeV, a discrete level structure is still present.

B. $^{58}\text{Ni} + ^{58}\text{Ni}$ reaction

A second experiment was performed by bombarding a $440 \mu\text{g}/\text{cm}^2$ thick ^{58}Ni target with a 240-MeV ^{58}Ni beam. This reaction produces the compound nucleus $^{116}\text{Ba}^*$ with an excitation energy ~ 63 MeV. The β -delayed proton emitter ^{113}Xe ($E_p \sim 2-7$ MeV, $t_{1/2} = 2.7$ s, $b_{\beta p} = 0.07$ [22]) should be produced in this reaction via the $2p_n$ channel. The strong channels for this reaction are ^{113}I ($3p$ [23]), ^{112}I ($3pn$), ^{112}Te ($4p$ [24]), and ^{110}Te ($\alpha 2p$ [25]). Figure 8 shows an $A = 113$ gated decay energy spectrum.

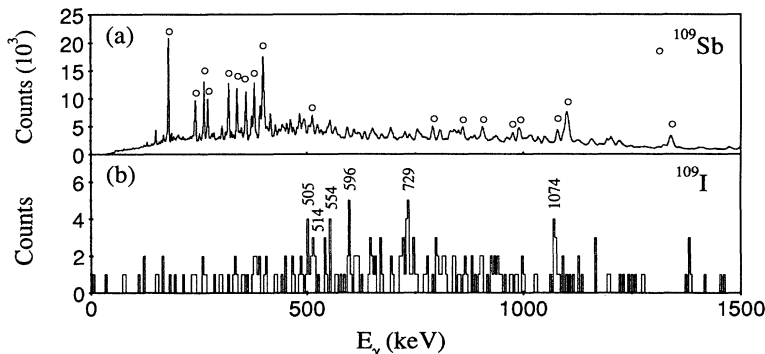


FIG. 7. (a) Mass-gated ($A = 109$) γ -ray spectrum with the strong transitions from ^{109}Sb indicated. (b) Gamma rays correlated with the proton decay of ^{109}I . The binning of spectrum (a) is 1 keV/channel while spectrum (b) has been compressed to 4 keV/channel.

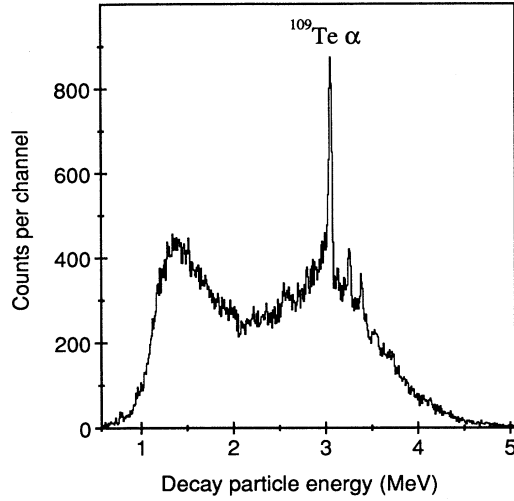


FIG. 8. Charged-particle decay energy spectrum gated for $A/q \approx 4.00$ which includes both $A = 113$ and 109 . The broad continuum which is the major part of the spectrum is from β -delayed proton emission from ^{113}Xe with $\sim 10\%$ contribution from β -delayed proton emission from ^{109}Te . The peaks are from known α decays, the strongest peak being the α decay of ^{109}Te .

In addition to the delayed protons from ^{113}Xe , there is also visible the alpha decay of ^{109}Te which arrives at the same place on the focal plane as a charge-state ambiguity. Consequently, there is a contamination of the ^{113}Xe delayed protons with ^{109}Te protons at a level of $\sim 10\%$. Figures 9(a)–9(c) show, respectively, the $A = 113$ gated γ rays, the decay-tagged γ -ray spectrum, and the resulting

TABLE III. Gamma-ray energies and intensities for transitions assigned to ^{113}Xe .

E_γ (keV) ^a	I_γ (%) ^b
415.7	100
520.4	20
525.9	25
600.7	15
607.8	25
656.0	75
826.2	70
940.7	60
1002.4	50
1066.2	35

^aEnergies are accurate to ± 0.5 keV.

^bIntensities are accurate to $\pm 15\%$.

subtracted spectrum showing γ rays from ^{113}Xe . Lines at 416, 656, and 826 keV are clearly visible in Fig. 9(c) and were not observed in the earlier ^{109}Te data. We therefore assign these transitions to ^{113}Xe .

Gamma rays in coincidence with the 416 keV transition are shown in Fig. 9(d) obtained from the recoil- γ - γ data ($A = 113$). A partial level scheme for ^{113}Xe is shown in Fig. 10. The 416-656-826-941-1002-1066 keV transitions appear to form a band structure. Two pairs of doublets (520/526 keV and 601/608 keV) are in coincidence with this band and are probably below the bandhead. A lack of clean gates precluded an unambiguous placement of these transitions. Furthermore, it was not possible to perform an angular correlation analysis for the ^{113}Xe transitions and the tentative spin-parity assignments in Fig. 10 are taken from systematics. The energies and intensities of the ^{113}Xe transitions are listed in Table III.

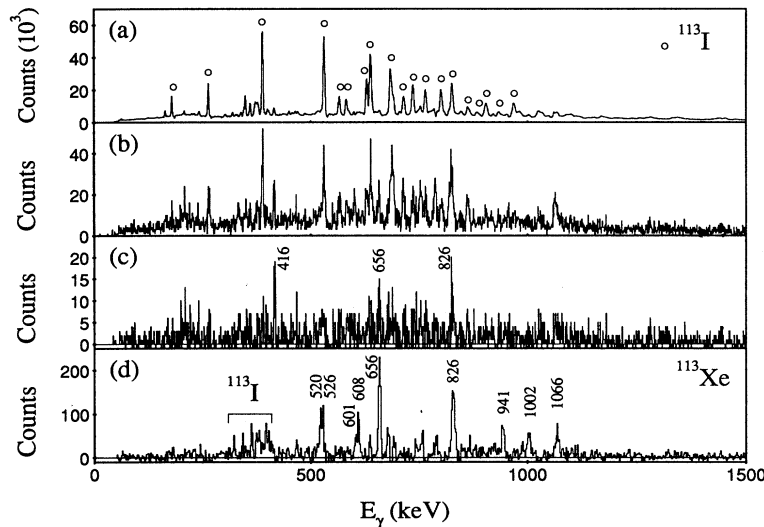


FIG. 9. (a) Mass-gated ($A = 113$) γ -ray spectrum with the strong transitions from ^{113}I indicated. (b) Gamma rays correlated with the β -delayed proton decay of ^{113}Xe . (c) Spectrum (b) minus a normalized fraction of spectrum (a) with the ^{113}Xe transitions labeled by their energies in keV. (d) Gamma rays in coincidence with the 416 keV transition obtained from a mass-gated ($A = 113$) γ - γ matrix. The transitions assigned to ^{113}Xe are labeled by their energies. A weak 416 keV transition also occurs for ^{113}I and the contaminating peaks are indicated. All other unlabeled peaks in (d) are contamination from $^{110,112}\text{Te}$. Furthermore, the intensity of the 1066 keV transition appears anomalously high since contaminating transitions of a similar energy occur in both ^{110}Te and ^{112}Te . The binning of spectra (a)–(c) is 1 keV/channel while spectrum (d) has been compressed to 2 keV/channel.

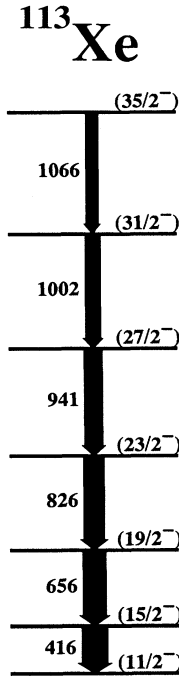


FIG. 10. Partial decay scheme for ^{113}Xe . Transition energies are given in keV and spin-parity assignments are tentative.

IV. DISCUSSION

A. Even tellurium systematics

The systematics of the ground-state bands of the even $^{108-124}\text{Te}$ isotopes ($N=56-72$) are shown in Fig. 11 [24–26]. The $E(4^+)/E(2^+)$ energy ratio is shown for each case. Values of 2.00 and 3.33 are predicted in the pure vibrational and rotational limits, respectively. The experimental values all lie close to the vibrational limit. The 2^+ and 4^+ states are at a minimum excitation energy for ^{120}Te ($N = 68$), reach a maximum for ^{114}Te ($N = 62$), and then decrease again for the most neutron-deficient isotopes. The 2^+ and 4^+ states in the even Te isotopes are understood as one- and two-phonon vibrational states [26]. The 6^+ and 8^+ states follow the same general trend. These states may represent three- and four-phonon vibrational states. It has also been suggested that two-quasiparticle $[\pi g_{7/2}^2]_{6^+}$ or $[\pi g_{7/2} d_{5/2}]_{6^+}$ configurations may couple to the zero- and one-phonon states of the spherical tin core to produce the observed 6^+ and 8^+ states [26]. The 6^+ state is particularly low lying for the heavier isotopes in Fig. 11. The 10^+ states steadily increase in excitation energy as N decreases and a maximum is reached for ^{112}Te . In addition to a possible five-phonon state, a $[\nu h_{11/2}^2]_{10^+}$ two-quasineutron configuration may explain the 10^+ states. Indeed, in some

Tellurium systematics

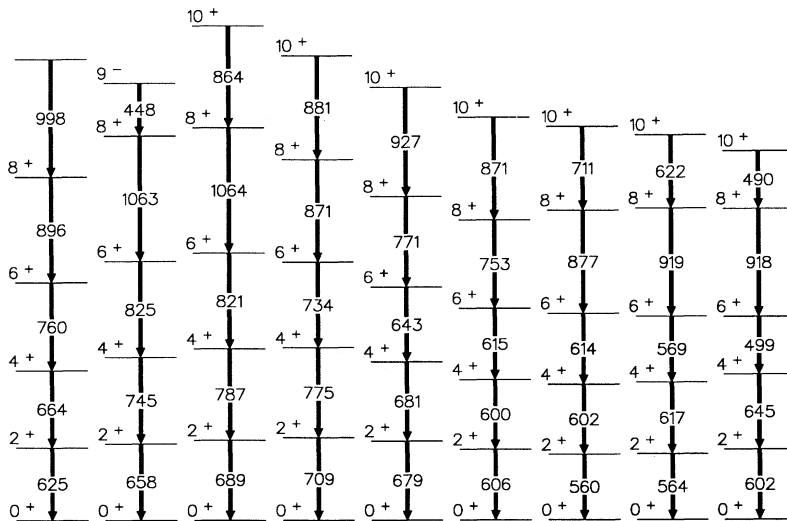


FIG. 11. Systematics of the ground-state bands in light even-even tellurium isotopes. $E(4^+)/E(2^+)$ energy ratios are shown for each nucleus. Energies are labeled in keV.

A : 108 110 112 114 116 118 120 122 124

$E(4^+)/E(2^+)$: 2.06 2.13 2.14 2.09 2.00 1.99 2.07 2.09 2.07

cases, more than one 10^+ state is observed ($^{114-120}\text{Te}$). No 10^+ state has been observed in ^{110}Te where odd-spin negative-parity states dominate the decay scheme for $I \geq 9$ [25]. This feature reinforces the $[\nu h_{11/2}^2]_{10^+}$ interpretation for the 10^+ states; by the time ^{110}Te is reached ($N = 58$), the neutron Fermi surface has fallen below the $\nu h_{11/2}$ subshell, making the two-quasineutron state energetically expensive. The highest level in ^{108}Te is therefore unlikely to be based on a two-quasineutron state. Instead, a vibrational five-phonon 10^+ state, or even a 9^- state similar to ^{110}Te , is more likely.

B. Odd- N ^{109}Te

Calculations based on the total-routhian-surface (TRS) formalism [27–29] for the light Te isotopes suggest weakly deformed prolate shapes with $\beta_2 = 0.12$ – 0.15 . At such deformations, a $d_{5/2}$ neutron state is at the Fermi surface for ^{109}Te and thus a ground-state spin and parity of $5/2^+$ are expected (this is also consistent with the proposed decay scheme of Fig. 6). The proposed $7/2^+$ state at the right of Fig. 6 is likely to be the unfavored signature component of the $d_{5/2}$ orbital. A $g_{7/2}$ neutron state is also near the Fermi surface, which could then be associated with the proposed $7/2^+$ state shown to the left in Fig. 6. A series of three transitions feeds this state. The low-spin yrast bands of odd- A Te isotopes with $A \geq 115$ are based on a $\nu h_{11/2}$ intruder orbital and hence the main (negative-parity) yrast sequence of ^{109}Te can also be associated with this orbital. In the heavier isotopes, the $11/2^-$ bandhead lies within a few hundred keV of the positive-parity ground state. However, in the ^{109}Te decay scheme, this $11/2^-$ state is 1090 keV above the ground state. This higher energy is again related to the position of the neutron Fermi surface which has fallen below the $\nu h_{11/2}$ subshell for the lightest Te isotopes. The high energy of the $11/2^-$ state in ^{109}Te allows it to decay to a lower $9/2^+$ state via a prompt $E1$ transition. In the heavier odd- A isotopes, the $11/2^-$ state is below the $9/2^+$ state causing the $11/2^-$ state to be isomeric and to decay via an $M2$ transition into the positive-parity states (i.e., $11/2^- \rightarrow 7/2^+$). The ^{109}Te ($N = 57$) level scheme is similar to the structures observed in odd- Z nuclei ($Z=53$ – 57) where the proton Fermi surface is at the bottom of the $\pi h_{11/2}$ subshell. In all cases, the low-spin yrast structures are associated with an $h_{11/2}$ “intruder” orbital.

Figure 12 shows the kinematic ($\mathcal{J}^{(1)} = I_x/\omega$) and dynamic ($\mathcal{J}^{(2)} = dI_x/d\omega$) moments of inertia for the $h_{11/2}$ yrast band of ^{109}Te . The $\mathcal{J}^{(2)}$ moment of inertia is quite irregular which indicates that ^{109}Te is not a good rotor. In particular, there is a large increase in energy for the 890 keV ($27/2^- \rightarrow 23/2^-$) transition. This behavior is normal for the low-spin structures of tellurium isotopes which are clearly not rotational; only recently has evidence been found for rotational structures in the tellurium isotopes, namely, for ^{112}Te [24] and ^{114}Te [30].

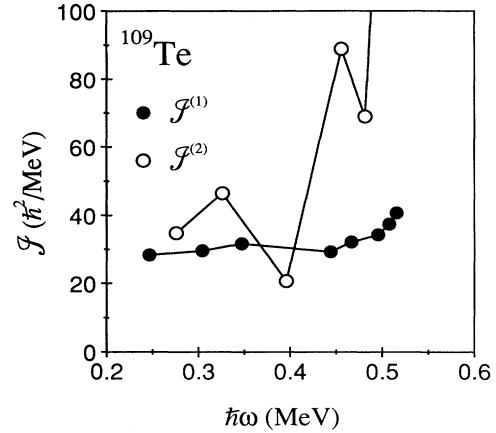


FIG. 12. Kinematic and dynamic moments of inertia for ^{109}Te plotted as a function of rotational frequency.

C. Odd- N ^{113}Xe

The structure of light odd- A Xe isotopes is quite similar to the odd- A Te isotopes. Low-lying $g_{7/2}$ and $d_{5/2}$ neutron orbitals are responsible for the ground states, while the high- j $\nu h_{11/2}$ intruder orbital dominates the yrast structure. Figure 13 shows the kinematic and dynamic moments of inertia for the proposed $h_{11/2}$ yrast band of ^{113}Xe (Fig. 10). Both moments of inertia vary more smoothly than for ^{109}Te (Fig. 12), indicating better rotational behavior for ^{113}Xe . This is expected since the xenon isotopes are further from the $Z = 50$ shell closure.

D. Odd- Z ^{109}I

Systematics of the $\pi h_{11/2}$ bands in odd- A iodine isotopes [23,31–34] are shown in Fig. 14, including the proposed ^{109}I structure. The energies of the $11/2^-$ bandheads are shown relative to the ground states (prolate

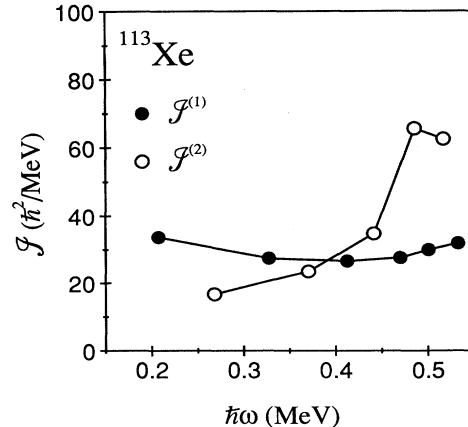


FIG. 13. Kinematic and dynamic moments of inertia for ^{113}Xe plotted as a function of rotational frequency.

Iodine systematics

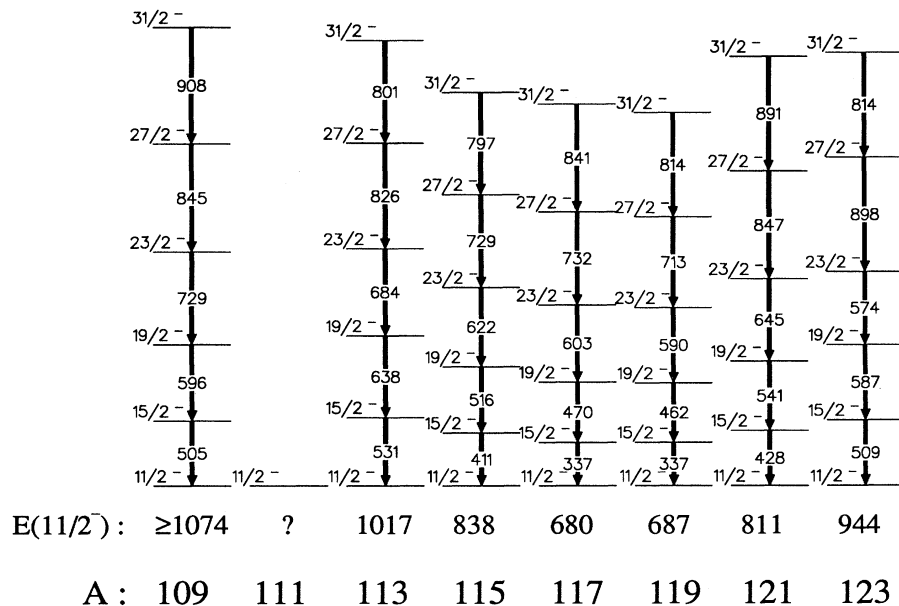


FIG. 14. Systematics of the $\pi h_{11/2}$ bands in odd- A iodine isotopes. The excitation energies of the $11/2^-$ bandheads are shown relative to the ground states ($5/2^+$) for each nucleus. Energies are labeled in keV.

$d_{5/2}$ states represent the ground states of $^{109-119}\text{I}$ while oblate $g_{7/2}$ states represent the ground states of $^{121,123}\text{I}$ [33]. The $15/2^-$ states are low lying for $^{117,119}\text{I}$, indicating maximum quadrupole deformation for these nuclei, before rising for the lighter isotopes, indicating decreasing deformation. However, similar to the 2^+ states in the lightest Te isotopes (Fig. 11), the $15/2^-$ state drops in energy for ^{109}I . This feature suggests a new onset of deformation for these extremely neutron-deficient nuclei. Indeed, this is also suggested from the ground-state proton decay characteristics of nuclei in this region such as ^{109}I and $^{112,113}\text{Cs}$, for which anomalously low spectroscopic factors may also indicate the onset of deformation, e.g., Ref. [35].

V. CONCLUSION

Transitions in $^{108,109}\text{Te}$, ^{109}I , and ^{113}Xe have been identified using the new technique of recoil decay tagging. In this method, the characteristic charged-particle radioactivity of very neutron-deficient nuclei has been used to select prompt γ -ray transitions recorded with the Eurogam spectrometer.

In the case of ^{109}I , we report the first observation of γ rays from a ground-state proton emitter despite the nonoptimal beam energy and current in this parasite

experiment. There is clearly great scope for extending the RDT technique to a multitude of nuclei decaying by charged-particle emission. It should be possible to study cases where one can select a cascade of γ rays feeding a particular state such as a high-spin radioactive isomer in a given nucleus. The RDT technique will increase in sensitivity with the advent of more efficient γ -ray arrays such as Euroball III [36] and higher efficiency recoil separators such as the Argonne Fragment Mass Analyzer [37]. Furthermore, with the development of radioactive ion beams with lower associated fluxes, the correlation of recoiling ions and decays will become increasingly sensitive. In summary, we believe that RDT can provide a useful tool for extending γ -ray spectroscopy into the region of, and beyond, the proton drip line and to high- Z nuclei.

ACKNOWLEDGMENTS

The Eurogam project is funded jointly by the Science and Engineering Research Council (U.K.) and IN2P3 (France). This work was also partly funded by the National Science Foundation. Two of us (R.M.C., S.A.F.) acknowledge receipt of SERC postgraduate studentships during the course of this work, while K.H. acknowledges support from York University.

- [1] C.J. Lister, M. Campbell, A.A. Chishti, W. Gelletly, L. Goettig, R. Moscrop, B.J. Varley, A.N. James, T. Morrison, H.G. Price, J. Simpson, K.A. Connell, and O. Skeppstedt, *Phys. Rev. Lett.* **59**, 1270 (1987).
- [2] G. Sletten, D. Foltescu, A. Johnson, J. Nyberg, H.A. Roth, D. Seweryniak, O. Skeppstedt, E. Adamides, S.E.

Arnell, A. Atac, J. Blomqvist, J. Cederkäll, B. Cederwall, C. Fahlander, H. Grawe, E. Ideguchi, R. Julin, S. Juutinen, W. Karczmarczyk, M. Karny, A. Kerek, J. Kownacki, T. Kuroyanagi, S. Mitarai, A. Nilsson, L.-O. Norlin, M. Piiparinen, R. Schubart, S. Törmanen, A. Virtanen, and R. Wyss, in *Proceedings of the Interna-*

- tional Conference on the Future of Nuclear Spectroscopy, Crete, 1993*, edited by W. Gelletly, C.A. Kalfas, R. Vlastou, S. Harissopulos, and D. Loukas (Institute of Nuclear Physics, NCSR Demokritos, Athens, 1994), p. 99.
- [3] A. Johnson, D. Seweryniak, B. Cederwall, J. Nyberg, A. Atac, J. Blomqvist, J. Cederkäll, C. Fahlander, M. Karny, A. Kerek, J. Kownacki, L.-O. Norlin, R. Wyss, E. Adamides, H. Grawe, E. Ideguchi, R. Julin, S. Juutinen, W. Karczmarczyk, S. Mitarai, M. Piiparinen, R. Schubart, G. Sletten, S. Törmanen, and A. Virtanen, *Nucl. Phys.* **A557**, 401c (1993).
 - [4] R.D. Page, P.J. Woods, R.A. Cunningham, T. Davinson, N.J. Davis, A.N. James, K. Livingston, P.J. Sellin, and A. Shotter, *Phys. Rev. C* **49**, 3312 (1994).
 - [5] P.J. Sellin, P.J. Woods, D. Branford, T. Davinson, N.J. Davis, D.G. Ireland, K. Livingston, R.D. Page, A.C. Shotter, S. Hofmann, R.A. Hunt, A.N. James, M.A.C. Hotchkis, M.A. Freer, and S.L. Thomas, *Nucl. Instrum. Methods A* **311**, 217 (1992).
 - [6] A.N. James, T.P. Morrison, K.L. Ying, K.A. Connell, H.G. Price, and J. Simpson, *Nucl. Instrum. Methods A* **267**, 144 (1988).
 - [7] C.W. Beausang, S.A. Forbes, P. Fallon, P.J. Nolan, P.J. Twin, J.N. Mo, J.C. Lisle, M.A. Bentley, J. Simpson, F.A. Beck, D. Curien, G. deFrance, and G. Duchêne, *Nucl. Instrum. Methods A* **313**, 37 (1992).
 - [8] P.J. Nolan, *Nucl. Phys.* **A520**, 657c (1990).
 - [9] V.P. Janzen, D.R. LaFosse, H. Schnare, D.B. Fossan, A. Galindo-Uribarri, S.M. Mullins, E.S. Paul, L. Persson, S. Pilotte, D.C. Radford, H. Timmers, J.C. Waddington, R. Wadsworth, D. Ward, J.N. Wilson, and R. Wyss, *Phys. Rev. Lett.* **72**, 1160 (1994).
 - [10] R. Wadsworth, H.R. Andrews, R.M. Clark, D.B. Fossan, A. Galindo-Uribarri, V.P. Janzen, J.R. Hughes, D.R. LaFosse, S.M. Mullins, E.S. Paul, D.C. Radford, P. Vaska, M.P. Waring, D. Ward, J.N. Wilson, and R. Wyss, *Nucl. Phys.* **A559**, 461 (1993).
 - [11] R. Wadsworth, H.R. Andrews, C.W. Beausang, R.M. Clark, D.B. Fossan, A. Galindo-Uribarri, I.M. Hibbert, K. Hauschild, J.R. Hughes, V.P. Janzen, D.R. LaFosse, S.M. Mullins, E.S. Paul, D.C. Radford, H. Schnare, P. Vaska, D. Ward, and I. Ragnarsson, *Phys. Rev. C* **50**, 483 (1994).
 - [12] F. Heine, T. Faestermann, A. Gillitzer, J. Homolka, M. Köpf, and W. Wagner, *Z. Phys. A* **340**, 225 (1991).
 - [13] D. Schardt, T. Batsch, R. Kirchner, O. Klepper, W. Kurcewicz, E. Roeckl, and P. Tidemand-Petersson, *Nucl. Phys.* **A368**, 153 (1981).
 - [14] D. Schardt, R. Kirchner, O. Klepper, W. Reisdorf, E. Roeckl, P. Tidemand-Petersson, G.T. Ewan, E. Hagberg, B. Jonson, S. Mattsson, and G. Nyman, *Nucl. Phys.* **A326**, 65 (1979).
 - [15] D.D. Bogdanov, V.A. Karnhavkov, and L.A. Petrov, *Sov. J. Nucl. Phys.* **17**, 233 (1973).
 - [16] P. Tidemand-Petersson, R. Kirchner, O. Klepper, E. Roeckl, D. Schardt, A. Plochocki, and J. Zylicz, *Nucl. Phys.* **A437**, 342 (1985).
 - [17] T. Faestermann, A. Gillitzer, K. Hartel, P. Kienle, and E. Nolte, *Phys. Lett.* **137B**, 23 (1984).
 - [18] P.J. Sellin, P.J. Woods, T. Davinson, N.J. Davis, K. Livingston, R.D. Page, A.C. Shotter, S. Hofmann, and A.N. James, *Phys. Rev. C* **47**, 1933 (1993).
 - [19] D.C. Radford, in *Proceedings of the International Seminar on The Frontier of Nuclear Spectroscopy, October, 1992, Kyoto*, edited by Y. Yoshizawa, H. Kusakari, and T. Otsuka (World Scientific, Singapore, 1993), p. 229.
 - [20] K.S. Krane, R.M. Steffen, and R.M. Wheeler, *Nucl. Data Tables A* **11**, 351 (1973).
 - [21] S. Hofmann, in *Particle Emission from Nuclei*, edited by D.N. Poenaru and M. Ivascu (CRC Press, Boca Raton FL, 1989), Vol. 2, Chap. 2.
 - [22] E. Roeckl, R. Kirchner, O. Klepper, G. Nyman, W. Reisdorf, D. Schardt, K. Wien, R. Fass, and S. Mattsson, *Phys. Lett.* **78B**, 393 (1978).
 - [23] E.S. Paul, C.W. Beausang, R.M. Clark, R.A. Cunningham, T. Davinson, S.A. Forbes, D.B. Fossan, S.J. Gale, A. Gizon, J. Gizon, K. Hauschild, I.M. Hibbert, A.N. James, P.M. Jones, M.J. Joyce, D.R. LaFosse, R.D. Page, H. Schnare, P.J. Sellin, J. Simpson, R. Wadsworth, M.P. Waring, and P.J. Woods, *Phys. Rev. C* **48**, R490 (1993).
 - [24] E.S. Paul, C.W. Beausang, S.A. Forbes, S.J. Gale, A.N. James, P.M. Jones, M.J. Joyce, H.R. Andrews, V.P. Janzen, D.C. Radford, D. Ward, R.M. Clark, K. Hauschild, I.M. Hibbert, R. Wadsworth, R.A. Cunningham, J. Simpson, T. Davinson, R.D. Page, P.J. Sellin, P.J. Woods, D.B. Fossan, D.R. LaFosse, H. Schnare, M.P. Waring, A. Gizon, J. Gizon, T.E. Drake, J. DeGraaf, and S. Pilotte, *Phys. Rev. C* **50**, 698 (1994).
 - [25] E.S. Paul, H.R. Andrews, V.P. Janzen, D.C. Radford, D. Ward, T.E. Drake, J. DeGraaf, S. Pilotte, and I. Ragnarsson, *Phys. Rev. C* **50**, 741 (1994).
 - [26] T. Lönnroth, A. Virtanen, and J. Hattula, *Phys. Scr.* **34**, 682 (1986), and references therein.
 - [27] W. Nazarewicz, G.A. Leander, and J. Dudek, *Nucl. Phys.* **A467**, 437 (1987).
 - [28] R. Wyss, J. Nyberg, A. Johnson, R. Bengtsson, and W. Nazarewicz, *Phys. Lett. B* **215**, 211 (1988).
 - [29] W. Nazarewicz, R. Wyss, and A. Johnson, *Nucl. Phys.* **A503**, 285 (1989).
 - [30] D.B. Fossan (private communication).
 - [31] E.S. Paul, R.M. Clark, S.A. Forbes, D.B. Fossan, J.R. Hughes, D.R. LaFosse, Y. Liang, R. Ma, P.J. Nolan, P.H. Regan, P. Vaska, R. Wadsworth, and M.P. Waring, *J. Phys. G* **18**, 837 (1992), and references therein.
 - [32] M.P. Waring, D.B. Fossan, J.R. Hughes, D.R. LaFosse, Y. Liang, R. Ma, P. Vaska, S.A. Forbes, E.S. Paul, R.M. Clark, and R. Wadsworth, *Phys. Rev. C* **48**, 2629 (1993), and references therein.
 - [33] Y. Liang, D.B. Fossan, J.R. Hughes, D.R. LaFosse, T. Lauritsen, R. Ma, E.S. Paul, M.P. Waring, P. Vaska, and N. Xu, *Phys. Rev. C* **45**, 1041 (1992), and references therein.
 - [34] R. Goswami, B. Sethi, P. Banerjee, and R.K. Chattopadhyay, *Phys. Rev. C* **47**, 1013 (1993), and references therein.
 - [35] R.D. Page, P.J. Woods, R.A. Cunningham, T. Davinson, N.J. Davis, A.N. James, K. Livingston, P.J. Sellin, and A.C. Shotter, *Phys. Rev. Lett.* **72**, 1798 (1994).
 - [36] J. Eberth, in *Proceedings of the International Conference on the Future of Nuclear Spectroscopy* (Ref. [2]), p. 397.
 - [37] C.N. Davids, B.B. Back, K. Bindra, D.J. Henderson, W. Kutschera, T. Lauritsen, Y. Nagame, P. Sugathan, A.V. Ramayya, and W.B. Walters, *Nucl. Instrum. Methods B* **70**, 358 (1992).